J. Condensed Matter Nucl. Sci. 39 (2025) 417–436

Research Article

Anomalous Heat Reaction from Hydrogen and Metals

Tadahiko Mizuno

Company Executive of Hydrogen Engineering Development & Application, Three System Build
6F, 1-15, Nishi4 kita12, Kita-ku, Sapporo 001-0012, JAPAN

Jed Rothwell

Librarian at LENR-CANR.org (cold fusion library), 3625 Woodstream Circle, Brookhaven GA 30319

Abstract

The author previously reported anomalous phenomena [1]–[5] in metal hydride systems. We assumed the phenomena was a typical nuclear fusion reaction, initially assuming it during electrolysis in heavy water solutions, so neutron generation was also measured [6]. Next, analysis was done of the isotopic change in elements produced during electrolysis tests. Anomalous excess heat (heat exceeding input energy) was generated during this experiment, but it was difficult to control [7]–[10]. In addition to Pd, anomalous heat has been reported mainly in Ni-H systems [11]–[14].
 ISSN 2227-3123

Keywords: Cold Fusion, Excess heat, SUS stainless reactor, Air flow calorimetry, Nickel film

1. Introduction

The author placed a cleaned Ni mesh as the reaction body up against the inner surface of a stainless-steel reactor. The reactor was then heated in an insulated chamber. The nickel internal gas was removed by heating and vacuum pump. Additionally, high voltage was applied to the electrodes inside the reactor, and the Ni surface was bombarded with electrons and ions to remove surface impurities. By this method, excess heat (heat output minus input greater than zero) equivalent to the heating power applied to the reactor was obtained. However, serious doubts arose during the testing process. The calibration heater used should not generate excess heat at all, yet in some cases it seemed that excess heat was generated when the heater was used in combination with an SUS reactor with an active surface. Calibration is not done by simply using the heaters as they are, but by placing them in variously shaped metal holders. It was assumed that excess heat could not come from such a heater alone, and an analysis was conducted. Some data that did not match the expected null result. As a result of detailed analysis, it was found that there was an abnormality in the reactor-reactor system used as a control. By changing calibration method and re-testing, it was found that stainless steel used for the control reactor that has been suitably treated will, under certain conditions, produce excess heat.

 ISSN 2227-3123

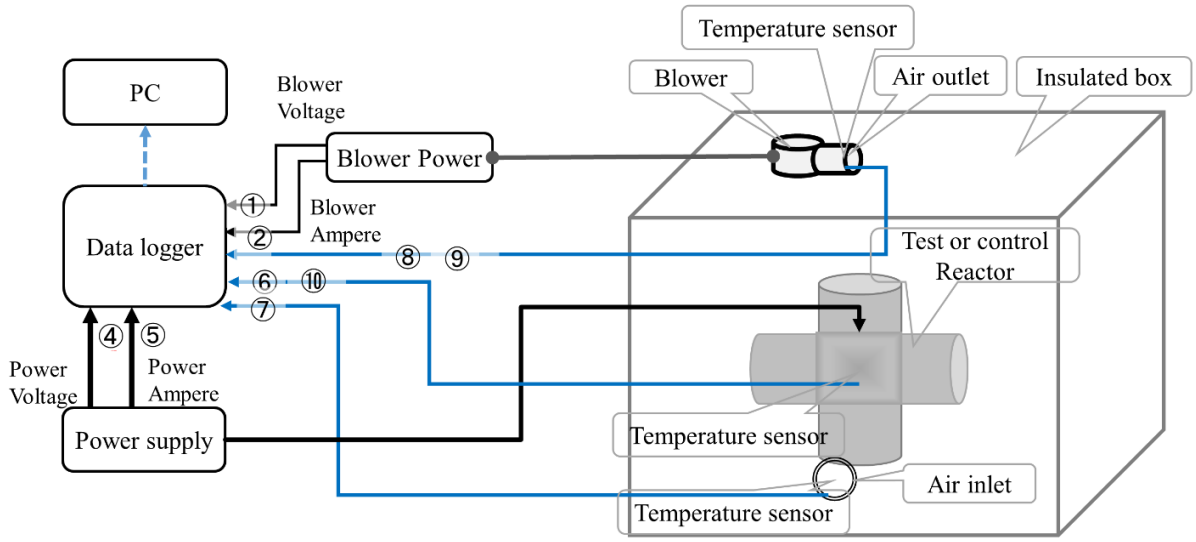

Figure 1. Schematic of measurement system.

2. Calorimetry

As described in a previous paper [15], air-flow calorimetry is used. As shown in the configuration in Figure 1, the reactor is placed in an insulated box (the calorimeter chamber), which has a constant flow of cooling air flowing in from an orifice at the bottom of the chamber and out from top orifice. The inlet air temperature is measured with an RTD. A fan is installed in the upper orifice, with another RTD and an air-flow meter. The reactor surface temperature is also measured at the hottest point on the reactor cylinder in the middle, and at the ends. The temperature at the ends is about 30% lower than the middle. Based on this, it is assumed that the reaction occurs in the middle portion. All data is collected by a logger and stored on an SD card.

Figure 1 shows the reactor box on the right, and the control system and measurement system on the left. Shown from the bottom left are: the power supply, a data logger (Graphtec, midi Logger GL840), and personal computer to record the data. Not shown in Figure 1 are diaphragm vacuum gauges (ULVAC, GCMT, G-TRAN, and ISG-1).

Figure 1 shows: the blower input voltage (1) and (2) amperage, (3) pressure, (4) input heater voltage $\times$ 24 (5) input heater amperage $\times$ 1.25, (6), the calibration reactor surface temperature measured with a K-type thermocouple, (7) calorimeter chamber air inlet temperature measured with a PT100 RTD, (8,9) chamber air outlet temperature measured with a PT100 RTD, (10) reactor surface temperature measured with a K-Type thermocouple. Values from each of these are recorded by the logger.

The air inlet is drawn at the bottom center of the figure, but the actual box has the center of the hole 10 cm from the bottom and 10 cm from the left.

Data is not collected directly from the anemometer into the logger, because the anemometer does not have a data port. Before the test, and after every change in the calorimeter configuration, the anemometer is tested by stepping the fan motor through several power levels, and by moving the anemometer probe across the face of the outlet. The fan power level correlates with the wind speed. During the test, this correlation is manually checked from time to time. The wind speed is read from the anemometer and compared to the fan power.

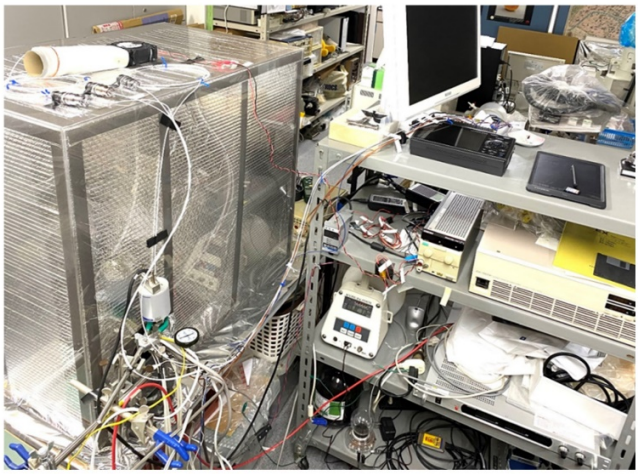

Figure 2. Calorimeter.

Figure 2 is a photograph of the calorimeter. The chamber on the left is an acrylic box with aluminum film and foamed polyethylene sheet bubble insulation on the inside. The thermal reflectance of aluminum is 0.94-0.98 at 1–10 micrometers, and it is 0.99 at 10 micrometers. [16] (reference: *Emissivity of aluminum and its importance for radiometric measurement, Measurement of physical quantities, J. Bartl and M. Baranek, pp. 31–36, 2004*). It is 800 mm long by 500 mm long, 700 mm high. An inlet hole 100 mm in diameter is in the lower left side of box, with an RTD. The outlet hole is in the top, center where an aluminum foil is attached to the inside of the air inlet to block radiant heat from the inside. Measurement instruments are shown on the right. The logger connection, fan power, and heater power supply wires are introduced from the top of the box. On figure 2 it seems many connections go through the lower corner. Figure 2-1 shows a close-up photograph of the hole.

The diameter of the hole is 100 mm, and the electric power input to the internal furnace body, the thermocouple for the temperature of the furnace body, the vacuum exhaust pipe inside the furnace body, etc. pass through the hole. In addition, the entire box is covered with a 10 mm-thick high-temperature glass insulation sheet on the desk and further covered with a 0.3 mm-thick aluminum reflector, which surrounds the bottom of the measuring box. Figure 2-2 shows the aluminum reflector and the corners of the box.

The logger collects data every 5 seconds. It collects the following: blower voltage and amperage, reactor gas pressure, heater input voltage and amperage, calibration reactor surface temperature, air temperature at the calorimeter chamber inlet (RTD), air temperature at the chamber outlet (RTD), reactor surface temperature (K-Type thermocouple). In a typical experiment, 10,000 to 20,000 lines of data are collected.

3. Calorimetry: The Ratio of Blower Input Power to Wind Speed

The thermal analysis is as follows. A circular pipe 200 mm long with a diameter of 66 mm (*The length of the pipe was 200 mm. The inner diameter is 66mm* is attached to the outlet of the blower, at the top of the calorimeter chamber. A circular pipe is used to ensure that the airflow speed is even at every point in the pipe cross section. An uneven air flow would complicate the calculation of the air volume. The fan is a sirocco type, which generates wind pressure of 20 to 30 Pa. This wind speed is high enough to ensure that the flow is turbulent, not laminar, according to the following

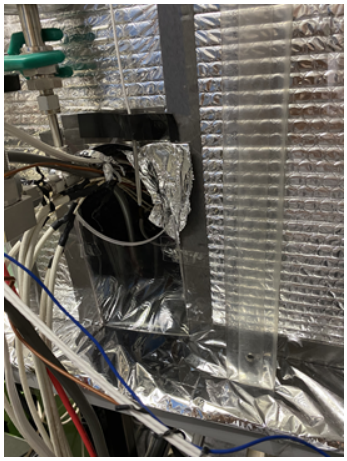

Figure 2-1. Enlarged photo of bottom hole.

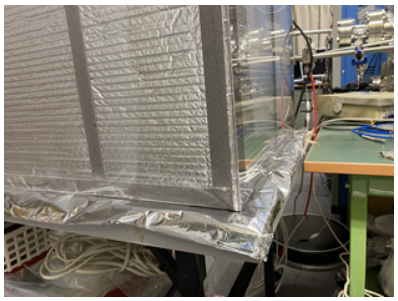

Figure 2-2. Reflective aluminum material placed under the box.

equation. The Reynolds number that separates laminar and turbulent flow is given by the following equation:

$$\mathrm{Re} = \rho \mathrm{UL}/\mu \tag{1}$$

Where:

ρ: Fluid density (kg/m^3) U: Average flow speed (m/s), L: length of pipe (m) (Pipe inner diameter)

μ: coefficient of viscosity (Pa · s) (physical property value)

If the Reynolds number is greater than 2300, the flow is turbulent; if it is smaller, the flow is laminar. Different textbooks cite somewhat different values; most are around 2300.

Air density ρ is 1.165 kg/m^3 at 30°C, U is wind speed 5 m/s, tube inner diameter is 0.066 m μ is 1.8×10^{-5} m^2/s. From this the Reynolds number Re is about 18,000, which is much larger than 2300, so it is definitely turbulent. Based on this, we can be confident that the flow velocity will be uniform in the pipe of the air outlet, and the air volume can be calculated accurately.

Air velocity is measured using a hot-wire digital anemometer (CW-60, Custom Co., Ltd.). This measuring instrument is temperature compensated and can accurately measure the air volume across a wide range of air temperatures.

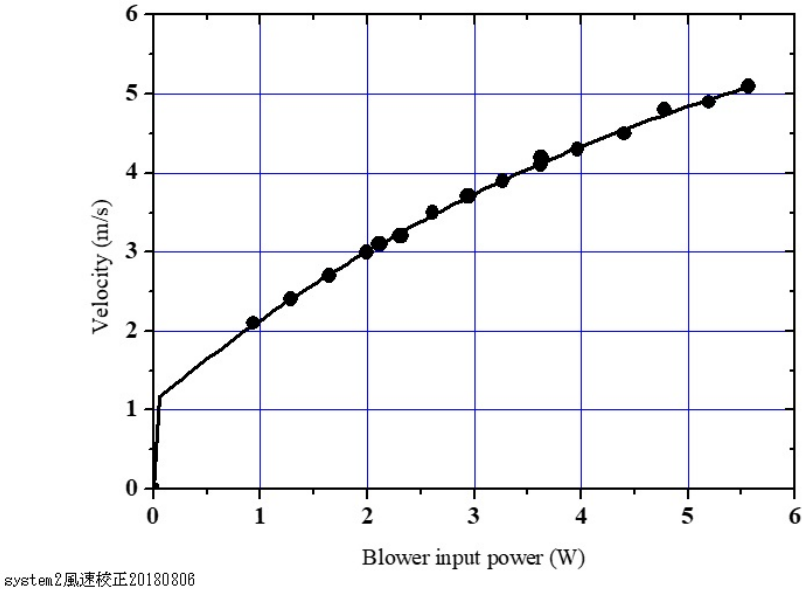

Figure 3. Relation between blower input power and wind speed.

The air flow rate was measured at different locations in the cross section of the outlet orifice. It was found to be uniform to within 0.1 m/s: it was 4.7 m/s both in center of the cylinder and close to the cylinder walls, including the walls at the top of the cylinder, and the bottom. Such close uniformity indicates that the flow is turbulent. The results shown in Fig. 13 were obtained at temperatures ranging from 24.2 and 24.9°C. Sufficiently accurate air temperature measurements at the inlet and outlet orifices are critical to the calorimetry. The thermocouples used in this study vary by 0.05 to as much as 0.3°C, so thermal calculations need to take that difference into account.

An RTD is use for low temperature measurements because it is more accurate than a thermocouple. An A-class Pt100 RTD is used (where 100 means the resistance is 100 ohms at 0°C), with a tolerance of $\pm$ (0.15 + 0.002|t|), where t is the absolute value of the temperature in degrees Celsius. With an air outlet temperature of 30°C, the error is about 0.2°C. An RTD has a significant thermal mass, so it takes 20 or 30 seconds to reach thermal equilibrium. The thermometer used in this study, 3.2 mm in diameter, takes 10 seconds to reach 90% of the equilibrium temperature in the stirred water.

The approximate formula for blower input power versus wind speed V obtained from Figure 3 is shown in equation (2): (*We are cumbersome, but we use this approximation. This is because the parameters are easy to understand because they are entered directly as numeric data.)*

$$\mathrm{V(m/s)} = y_0 + \mathrm{A}_1 \times (1 - \exp(-w_b/t_1)) + \mathrm{A}_2 \times (1 - \exp(-w_b/t_2)) \tag{2}$$

Where w_b is the blower input power. Constants are as follows: y_0: 3.42×10^{-12}, A_1: 1.1013, t_1: 0.00888, A_2: 6.308, t_2: 5.562

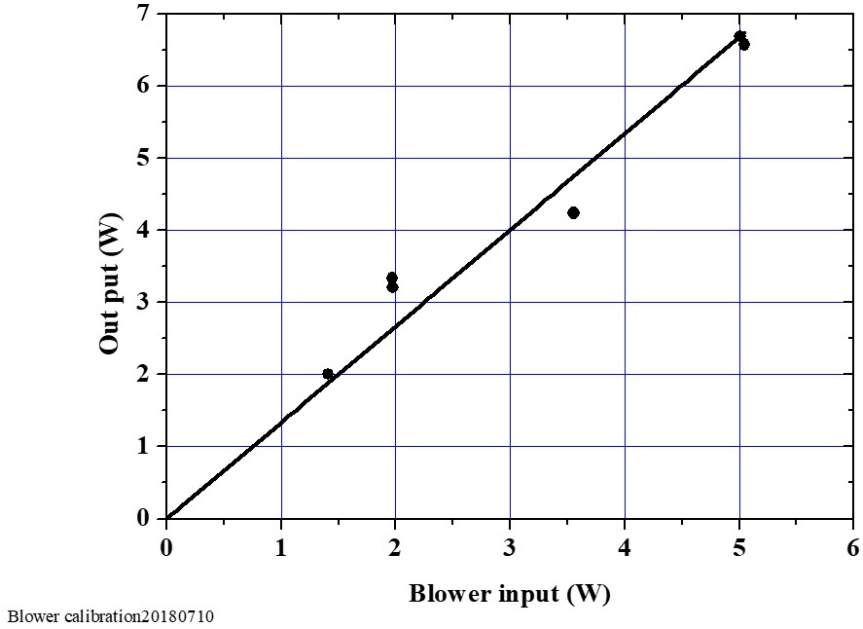

Figure 4. Energy added to the outlet air by the blower.

4. Relationship Between Blower Input and Air Outlet Temperature

When the blower is operated, the outlet air temperature rises from the heat of the blower. To measure the effect of the blower power on the outlet air temperature, blower power was varied and the change in temperature measured. During this test, there was no input power to the reactor. It was found that the outlet air temperature did rise measurably. As shown in Figure 4, the ratio of input power to the heat added to the air is almost a linear relationship. The slope of the straight line is 1.333. This heat from the blower is corrected for in the calorimetry.

This data is obtained by changing the blower input and measuring the temperature difference between the air outlet and inlet. The data was measured over 10 hours. At that time, looking at the input wattage, for example, 5-watt blower input, the heat output is about 6.7 W. It was thought that the temperature of the blower body rose when the blower was operated for a long period of time, and that heat contributed to the temperature of the air outlet.

Because of the conservation of energy, the heat output cannot be larger than the electrical input to the blower. In fact, the heat exported by the air must be lower than the electrical input because some energy is lost by the blower casing to the environment. An error of 1W on the input would be surprisingly high for electrical measurements. On the other hand, the error might be on the heat output value. It is proposed to modify the text as follows:

The heat output of this blower is subtracted and used for the calorimeter output power calculation. Figure 4 shows there is a discrepancy of more than 1 W between the blower input value and the heat output. This is because the input value of the blower is small, the output value is also small, and the error of the temperature detector is large. Calibrations with resistance heaters at much higher power levels show relatively smaller errors. The error is largest when measuring low power.

In fact, to correct the output power calculation it would be simpler and more correct to subtract the blower input energy rather than the output given on figure 4. In any case this modification is small.

5. Calorimetry: Heat Measurement

The heat measurement calculation is as follows. The constant pressure specific heat Cp is approximately represented by formula (3). It is affected by temperature. The effect of temperature on the air is discussed below in another example. In typical measurements, the room temperature was 293 K and the maximum air outlet temperature was 333 K. In this case, the heat capacity of the warmed air increases by 0.3%. The temperature dependence of the air heat capacity is linear with the temperature in the range of temperatures measured in these experiments. The coefficients of the first and second terms in equation (3) are constants, and $\mathrm{T_{out}}$ is the air outlet temperature. These temperatures are measured continuously at both the air inlet and outlet. However, the effect of the coefficient is 1/10 or less of the measurement error described below.

$$\mathrm{C_p} = 987 + 0.0661 \times \mathrm{T_{out}} : \mathrm{Jkg} - \mathrm{1K} - 1 \tag{3}$$

The input W_{total} is calculated by the formula (4).

$$W_{\mathrm{total}} = \sum_{0}^{T} (\Delta W + \Delta W b) \times \Delta t = \int_{0}^{T} (Wt + Wb)dt \tag{4}$$

Here, ΔW and ΔW_b are the electric power to the reactor and blower during the test, and Δt is the data sampling time interval.

The heat output H_{out} is obtained by equation (5).

$$H_{\mathrm{out}} = \sum_{0}^{T} \Delta V \times S \times \rho \times \mathrm{Cp} \times \Delta t = \int_{0}^{T} V \times S \times \rho \times \mathrm{Cp} \times \mathrm{dTdt} \tag{5}$$

Here V is the wind speed (m/s), S is the cross-sectional area of the air outlet (m^2): 3.42×10^3, and ρ is the air density (kg/m^3), which is expressed by Equation (6).

$$\rho = 3.40 \times \exp(-T_{\mathrm{out}}/201.26) + 0.415 \tag{6}$$

The wind speed V is experimentally approximated and expressed by the following equation, which will be repeated.

$$V(m/s) = y_0 + \mathrm{A_1} \times (1 - \exp(-w_b/t_1)) + \mathrm{A_2} \times (1 - \exp(-w_b/t_2)) \tag{7}$$

where the constants are y_0: 3.42×10^{-12}, $\mathrm{A_1}$: 1.10, t_1: 0.0089, $\mathrm{A_2}$: 6.31, t_2: 5.56. W_b in equation (4) is the blower input (Watt). In equation (5) *dT* is the temperature difference between the air inlet and outlet; $(T_{\mathrm{out}} - T_{\mathrm{in}})$. V is then represented by the blower input w_b.

$$V(\mathrm{m/s}) = 3.42 \times 10 - 12 + 1.10 \times (1 - \exp(w_b)/0.0089)) + 6.31 \times (1 - \exp(-(w_b)/5.56)) \tag{8}$$

From this, the weight of air is computed as follows:

$$M_A = \mathrm{Air\ weight/kg/s} = (V) \times 0.00264 \times (3.40 \times \exp(-T_{\mathrm{out}}/201.26) + 0.415) \tag{9}$$

Where *V* is the wind speed at the blower outlet, and T_{out} is the outlet air temperature in Kelvins. The corrected amount of heat in the outlet air CW_{out}(W) is as follows:

$$\mathrm{CW_{out}}(W) = (T_{\mathrm{out}} - T_{\mathrm{in}}) \times (C_p) \times (M_A) \tag{10}$$

Although atmospheric pressure change is also included in the heat calculation, it is confirmed that there is only a contribution of about 0.02% between 98.0 and 102.0 hPa. For each day, we used data released every hour from a weather station in Sapporo. The standard pressure is 101.3 hPa, and the daily variation is 101.0∼101.5 hPa, which is a variation of 0.5%. There is a pressure term in the spreadsheet, which we use in the heat calculations.

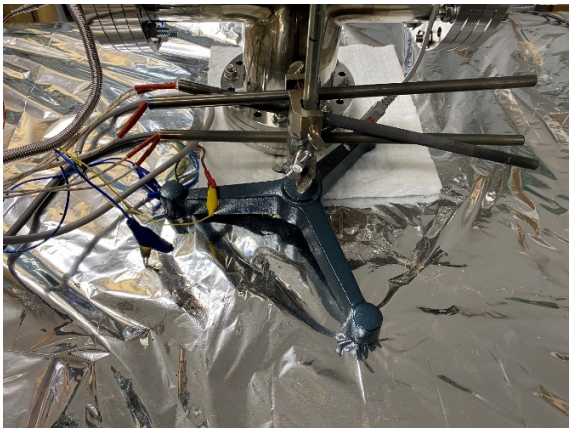

Figure 5. Three resistance heaters used to calibrate, mounted on a stand. The stand is shown here in the calorimeter chamber placed in front of a reactor. The stand is periodically moved around, and the heaters are moved up or down the pole, to confirm that moving the heat source does not affect the calorimetry.

Calculated as an ideal gas with pV=nRT.
From V=nRT/p, and then , ΔV=nRT/Δp
Therefore, equation (10) is approximately changed next equation.

$$CW_{\mathrm{out}}(W) = (T_{\mathrm{out}} - T_{\mathrm{in}}) \times (C_p) \times (M_A)/p/p_0.$$

where p_0 is 101.3 hPa.

6. Calibration Method

Three resistance heating elements, diameter 15 mm, length 200 mm, weight 300 g, were used to calibrate the calorimeter (Figure 5). They were mounted on a stand. To ensure the position of the heaters has no significant effect on the calorimetry, the stand was moved horizontally to different locations in the chamber, and the heaters were moved up and down the pole. When the heaters were run at a given power level, the position of the heaters did not measurably affect the outlet air temperature. Test reactors are always placed in the same position in the center of the chamber, to avoid any possible positional errors, even though moving the heating elements and running them at the same maximum power as the reactors shows there are probably no positional errors.

During the tests for excess heat, the reactors are heated with internal resistance heaters, not the three external heaters used to calibrate. (Except for Reactor R40, which is heated externally.)

The resistance heaters are run at different power levels, for 1 to 3 hours at each level. For example, the data points in Figure 7 were taken over two days in November 2022, with the power stepped through 100, 200, 300, 400, 500 and 600 W (Table 1). Data is recorded in spreadsheets. The average temperature difference (outlet temperature minus inlet) and air flow rate is measured at each step. This is done after the temperature stabilizes, after stepping up or down the power level. This takes about 30 minutes. Unfortunately, the room in which these tests are conducted is poorly insulated; it has no central heating; and it is in Sapporo, Japan where winter is cold, so inlet air temperatures vary a great deal. This introduces a lot of noise. To reduce noise, the average temperature was measured after the temperature stabilizes and during times when input temperature fluctuations are minimal, as shown in the red arrows in Figure 6. The standard deviation is measured to ensure the noise is low during these times.

Table 1. Six calibration power levels measured in November 2022.

Average calibration power (W)	Standard deviation	Average temperature difference (Outlet-Inlet) (°C)	Standard deviation
98.75	0.06	5.09	0.16
199.27	0.04	11.16	0.22
299.66	0.07	17.34	0.12
400.31	0.20	22.60	0.20
501.24	7.18	27.59	0.19
603.47	0.17	33.96	0.24

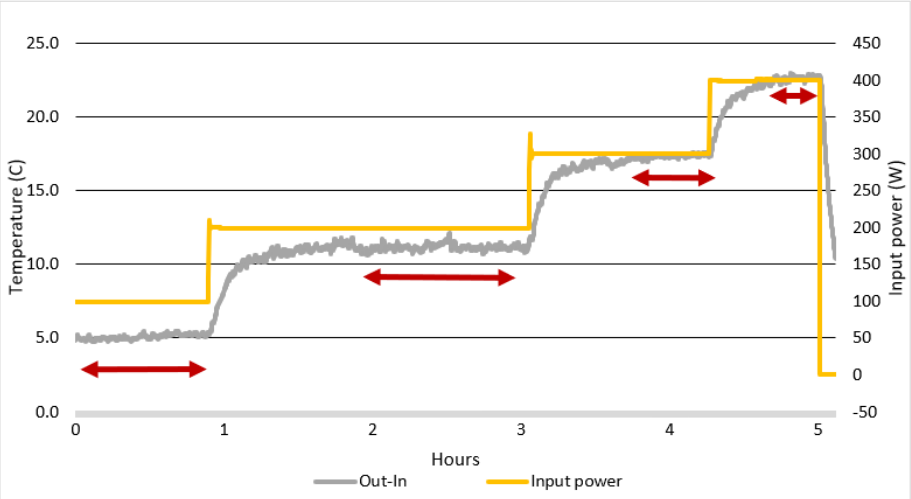

Figure 6. Calibration steps 100, 200, 300 and 400 W. The red arrows show when the temperature stabilized, and input fluctuations are at minimum. Average power and the standard deviation were measured during these times (see Table 1).

This calorimeter has been calibrated many times, over many years. Changes in the calibration constants have been small.

The calorimetry shows that not all heat is recovered in the flow of air. Some escapes from the walls of the calorimeter chamber. IR cameras show that the walls are warmer than the surroundings. The complex equation in the above section, "Calorimetry: heat measurement" shows that during a calibration with 0.603 kW, 0.395 kW are captured in the flow of air, and 0.208 kW escape from the chamber. This is shown in the sixth point in Figure 7.

A simpler analysis confirms this. During the 0.603 kW calibration, after the temperature stabilizes, the average outlet minus inlet temperature was 33.96°C (standard deviation 0.24). The wind speed during this segment of the test averaged 4.187 m/s (standard deviation 0.003). The mass of air passing through the outlet orifice was 0.012 kg/s. The specific heat of air at a constant pressure (isobaric) is 1.008 kJ/kg per degree K at 333 K. Thus, the airflow removed 0.405 kW of heat, and 0.198 kW escaped from the chamber walls. This is in reasonable agreement with the complex equation.

The temperature difference is between the outlet and inlet temperatures. Heat losses depend on the temperature difference, the greater the difference, the larger the heat losses, regardless of the weight or shape of the calibration heater. As shown in the graph, a difference of 10°C results in 52 W_{loss}; 20°C a 115 W loss, 30°C a 185 W loss. The amount of heat loss in this graph (shown as E_{loss} instead of W_{ex}) is approximately estimated in Eq. 11 as a function

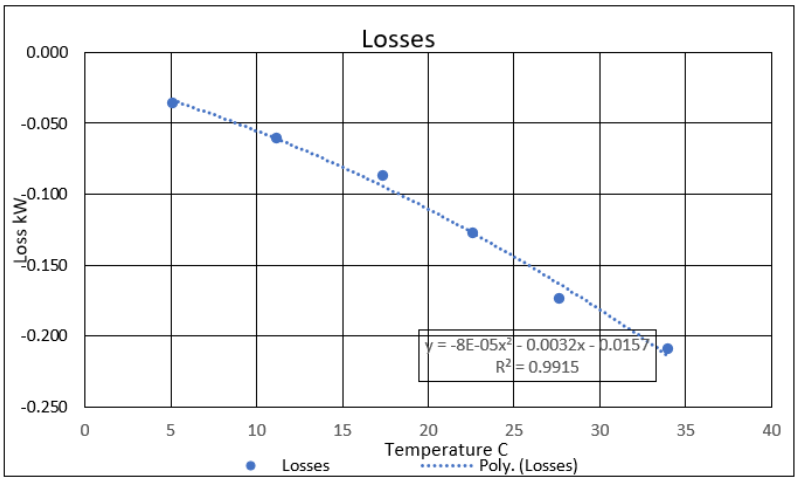

Figure 7. Energy loss from chamber. Horizontal axis: temperature difference between air outlet and inlet; vertical axis: energy loss. The trendline is a 2-order polynomial.

of the temperature difference *tk*.

$$E_{\text{loss}}/W = -132 \times (\exp((t)/36.2)) + 117 \tag{11}$$

The amount of heat generated is obtained by estimating the heat loss based on Equation 11, and adding the lost heat to the measured heat. As shown in the following equation (12).

$$(T_{\text{out}} - T_{\text{in}}) \times (Cp) \times (M_A) - (-132 \times (\exp((t)/36.2)) + 117) \tag{12}$$

7. Test Reactor R40

A schematic of the test reactor designated "R40" is shown in Figure 8. This reactor is made of SUS304 pipe. The length is 400 mm, diameter is 100 mm. The weight is 2 kg. A sheath heater of 100 V, 600 W is wrapped around the reactor. The reactant is a 27 g nickel mesh, 300 mm square. The reactor is evacuated, then filled with hydrogen gas at 1000Pa. Figure 9 is a photograph of reactor R40.

Three heaters of 300 mm in length, 12 mm in diameter, 120 g in weight, and 600 W are used for calibration. The heating element volume is 3 × 34 cm3 = 102 cm3. In practice, the calibration test removes the reactor body and tests only the heater. The positions of the calibration heaters are changed inside the box: top, bottom, right, left, back, and front. This is to investigate how heat escapes and the effects of thermal radiation. In the test, the input is 100 W, 200 W, and the temperature reached is 170 to 200°C and 350 to 400°C.

In the reactor test, a sheath heater, manufactured by Three High Co., Ltd., 100 V, 600 W, heat resistance 700°C, thickness 3.6 mm, length 300 cm, is wrapped around the outer periphery of the reactor. The heater volume in this case is 30.5 cc, which is smaller than the calibration heater.

In a typical reactor body test, the input is 100 to 150°C at 100W and 200 to 300°C at 200W, although it varies depending on the furnace body. At 600–700W, it is 300–400°C.

As a result, since three calibration heaters are used, the temperature rise of each heater can be suppressed, and the calibration test can be performed at a temperature close to the actual reactant temperature.

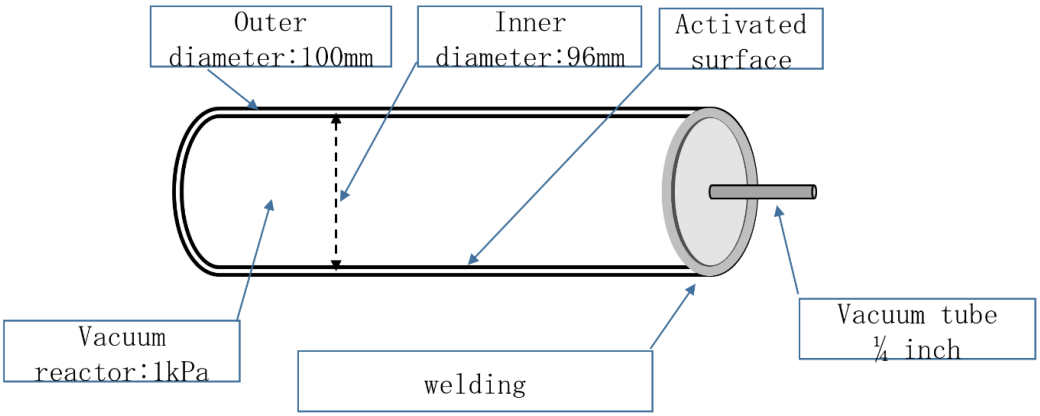

Figure 8. Test reactor R40.

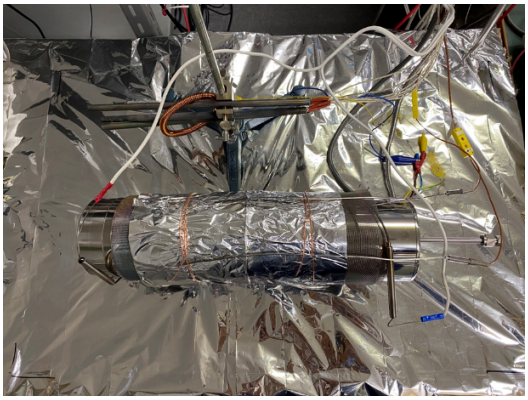

Figure 9. Reactor R40, placed in the calorimeter chamber near the air inlet.

In addition, the temperature of the radiation is 300 to 500°C, and the wavelength of the emitted far-infrared rays is much longer than 1 μm, and 100% of it is reflected by the aluminum film to heat the air inside the box.

8. Test Results

Excess heat results from reactor R40 are shown in Figure 10 and Figure 11. Input power is 100 W. Power out is 77 W, based on Eq. 10, not taking into account heat losses from the calorimeter chamber. Output corrected for heat losses is 115.1 W. Figure 11 shows tests with 601 W and 204.8 W. At 601 W, corrected output reaches 688.7 W. The output/input ratio is 688.7 W/601.0 W = 1.15. This ratio is not a fixed physical quantity, or an absolute measure, but only a rough indication of potential quantity, because it varies depending on the shape of the reactor, the insulation,

Table 2. Nominal low and high input power levels, and lowest and highest excess heat from reactors used in this study. All but R35 produced excess heat. Results are corrected for heat losses from the calorimeter chamber.

Reactor	Low input power (W)	High input power (W)	Low excess heat (W)	High excess heat (W)	Low ratio	High ratio
R40	100	600	15	100	1.15	1.15
R37	50	600	1.78	126	0.998	1.282
R8	101	493	11.5	127	1.114	1.257
R36	67	753	-2.6	285	0.978	1.379
R35	99	300	-27.13	1.81	0.897	1.005

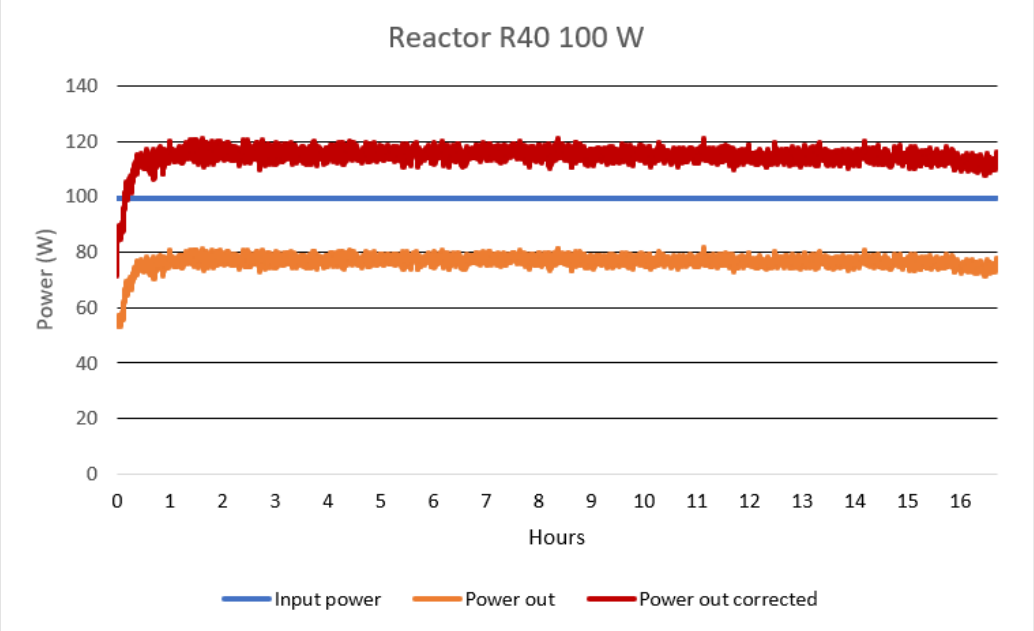

Figure 10. Reactor R40 heat production with 100.0 W of input. Blue line: input power. Orange: output heat not taking into account heat losses; Red: output heat taking into account heat losses from the calorimeter chamber.

and the air flow rate. However, the physical quantity of heat does depend on one important parameter: the temperature of the reactor.

The lowest and highest input and output nominal power and ratios for the five reactors in this study are shown in Table 2.

Figure 12 shows the reactor temperature and excess heat release. The horizontal axis is the temperature in degrees Celsius, and the vertical axis is the excess heat (W_{ex}) in watts. The temperature of the outer wall of the reactor body is shown in this graph, but it is known that the temperature of the reactor body varies across the surface. The center of the cylinder is at the highest temperature. For example, the heater is installed inside the cylinder at the center, so the temperature on the outside of cylinder around the center is 290 to 330°C. At the edge of the cylinder, away from the heater, the temperature drops to 200°C. The temperature inside the reactor body is estimated to be about 340°C. The relationship between temperature and W_{ex} can be approximated with an exponential function. Also, this value has a linear relationship with the Arrhenius plot as shown on the right side of the figure 13.

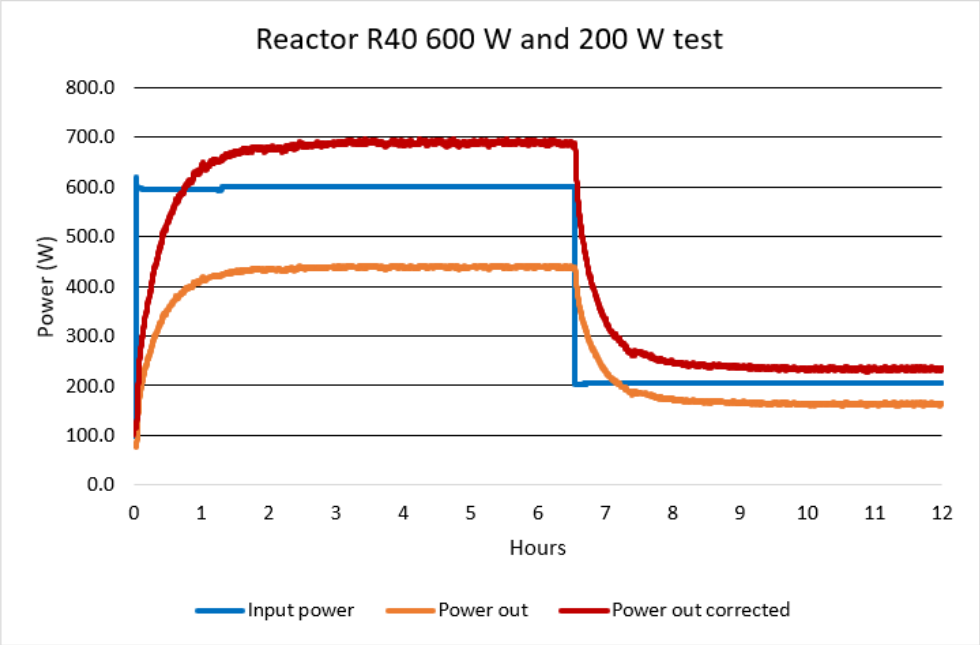

Figure 11. Reactor R40 heat production with 600 W and 200 W of input power. Orange line: output not taking into account heat losses; Red: heat taking into account heat losses from calorimeter chamber.

Although the ratios are not fixed physical quantities, Figure 14 shows the reactor temperature and output/input ratio for reference. It can be seen that the ratio does not depend much on the reactor temperature, being about 1.15 at any temperature. As shown in Figure 7, when the input is increased and the reactor temperature rises, the heat loss from the chamber increases exponentially, so the reactor temperature does not rise. We assume that to increase this ratio, the insulation around the reactor itself should be increased.

Output heat only exceeds input power when you take into account heat losses from the calorimeter chamber. On the other hand, it is higher than heat recovered during calibration. This can be shown with the temperature data alone, before converting it into heat. Figure 15 shows the outlet minus inlet air temperatures with Reactor R36, and with a calibration. During the stable periods shown with the red arrows, input power to R36 was 504 W (0.13 standard deviation), and 501 W (standard deviation 0.11) to the calibration. Outlet minus inlet temperatures were 31.7°C (standard deviation 0.18) for R36 and 27.5°C (standard deviation 0.17) for the calibration. The 4.1°C increase can be measured with confidence.

(The temperature reached equilibrium faster with the calibration because the thermal mass of heated metal is smaller, 20 kg versus 0.9 kg. The blue arrow points to the effect of an abrupt 1.4°C fall in inlet air temperature.)

Figure 16 shows the R36 result converted to heat, measured without correction for heat losses, and again with corrections. The extra 4.1°C in Figure 15 translates 598 W corrected, which exceeds the 504 W input power.

Figure 17 is an Arrhenius plot of excess heat per unit of reactor surface area (W_{ex}/cm^2) from each type of reactor body, of four different shapes.

R36: a cross-shaped reactor designed as a vacuum chamber, made of SUS304, 400 mm in length and width. Weight 20 kg, with the cylinder diameter 110 mm. There is a discharge electrode installed inside: a nickel wire with a diameter

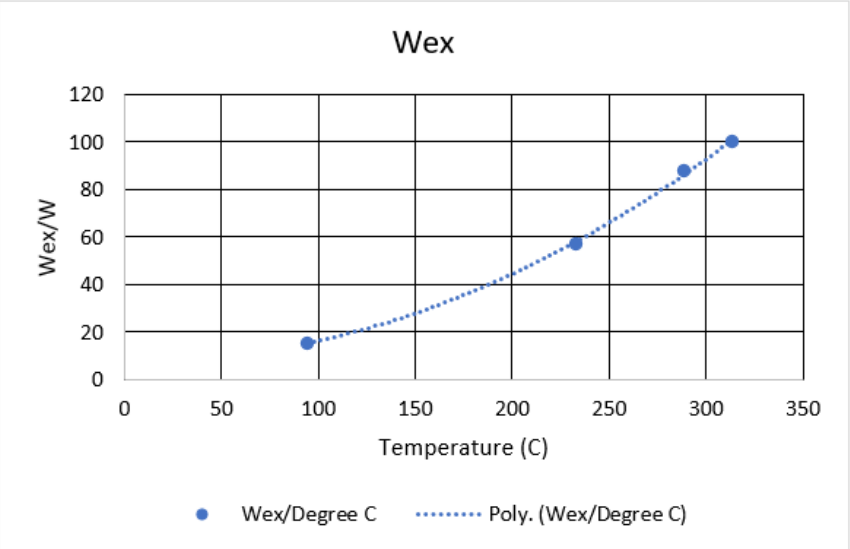

Figure 12. Reactor R40 temperature and excess heat production Wex.

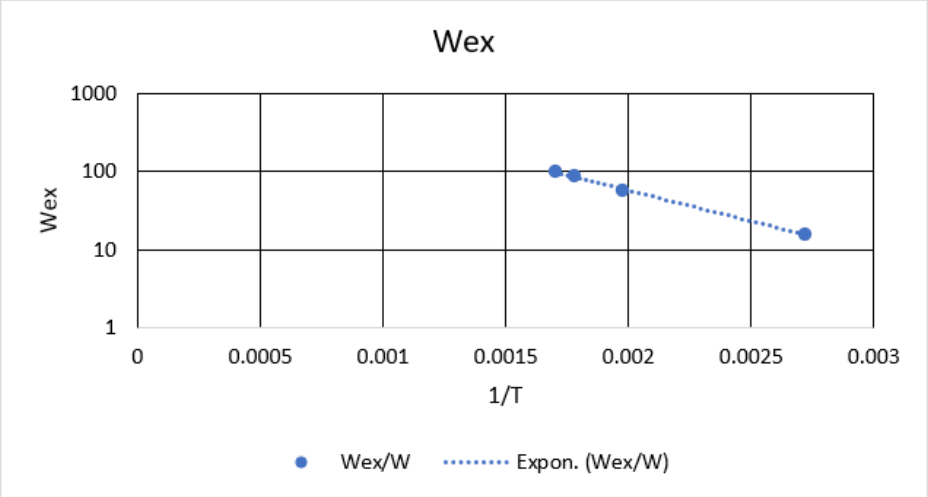

Figure 13. Reactor R40 Wex, expressed as the reciprocal of absolute temperature (Arrhenius plot).

of 1 mm φ and a length of 1000 mm, wound 30 times, with a diameter of 10 mm. A 100 V, 600 W, 700°C heat-resistant ceramic heater made by Three High Co., Ltd. is wrapped around the outside of the reactor.

Reactor R8: a cross-shaped reactor designed as a vacuum chamber, made of SUS304, 400 mm in length and width. Weight 20 kg, with the cylinder diameter 110 mm. There are two discharge electrodes inside the Weight 20.35 kg.

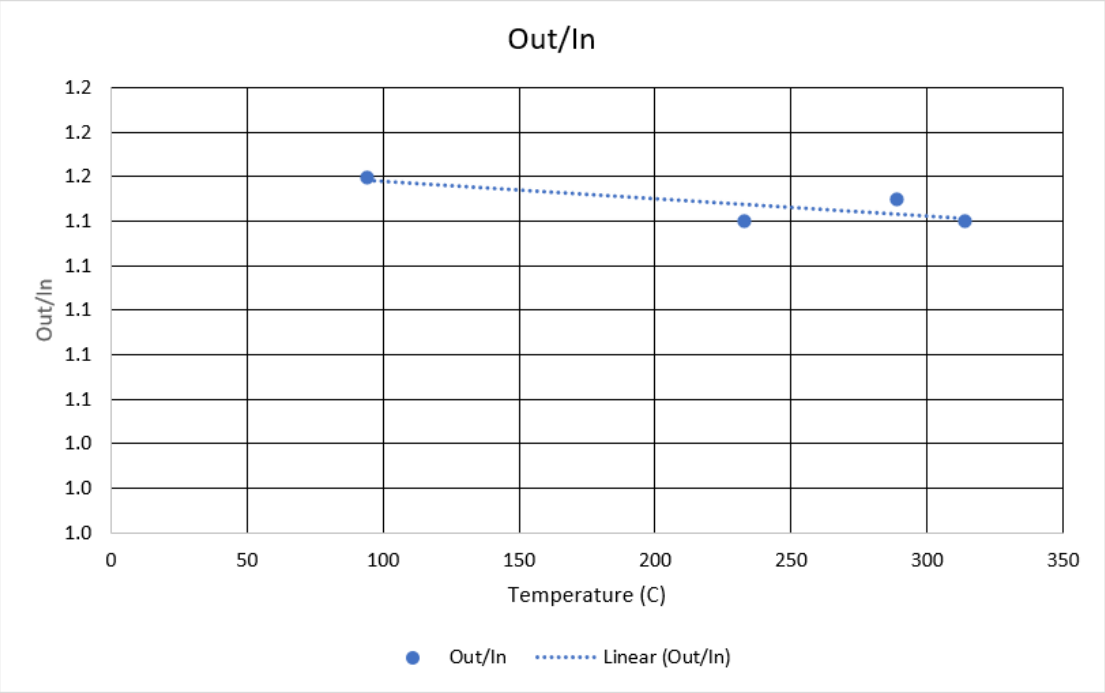

Figure 14. Reactor R, temperature, and output/input ratio.

Reactor R35: designed as a vacuum chamber. Length 300 mm, diameter 70 mm, ICF70 flange, weight 1478 g. The heater was used directly for calibration. After processing once, the reactor was opened. This reactor has no discharge electrode. Including the bottom cap (335 g), the valve is 270 g, the reactor weight is 873 g, and the volume is 300 cm^2. Before use, the inside of the reactor was washed with alcohol and then evacuated.

Reactor R37: This is an open SUS tube. The inner surface is mirror-finished. The tube length is 400 mm, the diameter is 110 mm, and the weight is 7 kg. A 600 W sheath heater is wrapped around the outer wall of the reactor body 10 times at equal intervals. The heater length is 3 m. There is no reactant metal inside the reactor body.

In Figure 17, the horizontal axis is the reciprocal of absolute temperature, 1/T. From this graph, the activation energy can be calculated from the slope of the straight line. Here, the data R40 this time shows a smaller value than R8. The activation energies are -0.23 eV/K/atm for R40, -0.287 eV/K/atom for R36, -0.268 eV/K/atm for R8, and -0.29 eV/K/atom for R37. These values are 1.4 to 1.7 times greater than 0.165 eV/K/atom for the larger reactor (50 kg weight). The frequency factor $W_{ex}0$ is R = 2.2 W, R37 = 90 W, R8=3 W, R3 = 7 W.

The diffusion activation energy in nickel is -28.6 kJ/mol, or -6.875 kcal/mol, so -0.298 eV/atom. This value is very close to the activation energy obtained above. The amount of dissolved hydrogen in nickel [17] is presumed to be an important factor for excess exothermic energy.

It has been found that hydrogen free radical generation reaction occurs in SUS that does not contain any contamination, such as metal atoms at a low temperature of 500°C or less, is due to the catalytic action of an ultra-clean metal surface [18].

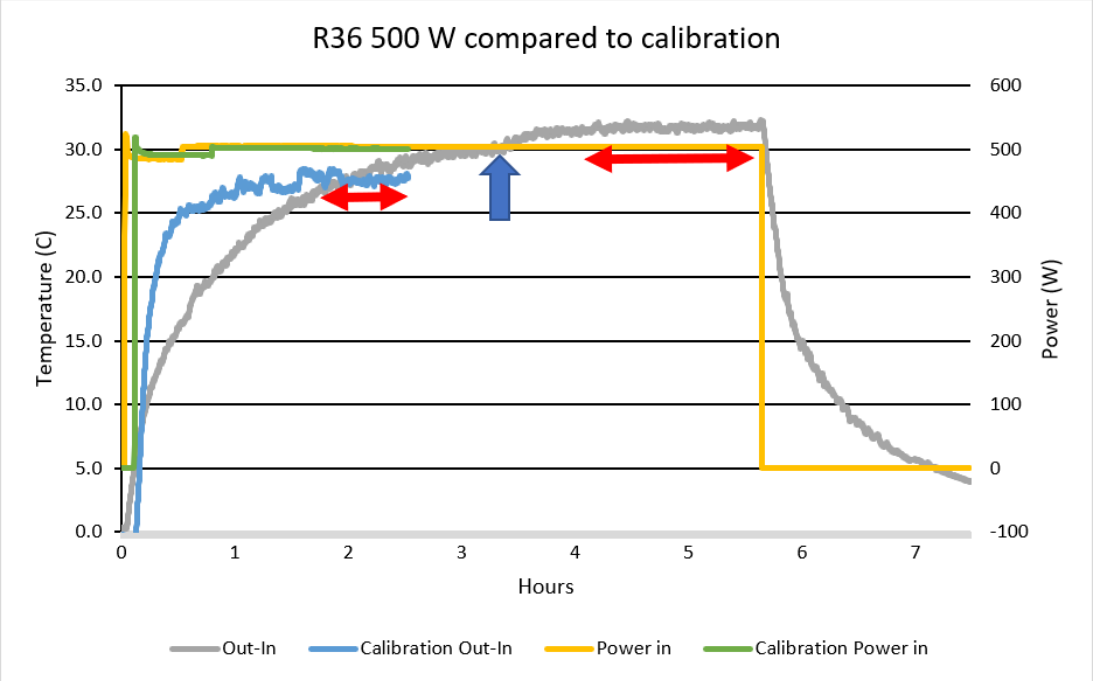

Figure 15. Reactor R36 500 W temperature compared to calibration. Stable periods shown with the red arrows. The blue arrow points to the effect of an abrupt 1.4°C fall in inlet temperature.

It has been found that this reaction is enhanced by heating to about 500°C. On a clean SUS surface, a unique hydrogen radical reaction occurs, so it is presumed that the moisture in the air is changed into hydrogen radicals, and this is related to the excess heat generation. Even without a special supply of hydrogen from the outside, there is always the presence of H_2O in the environment, and this hydrogen may cause the reaction to continue.

It is also reported that only hydrogen gas is generated from water by mechanical movement in a SUS ball mill. Since no oxygen was observed in this case, it has been speculated that iron is oxygen scavenging [19]. We presume oxygen scavenging is involved in hydrogen uptake into the metal because the processing of the SUS surface is a major factor causing excess heat generation.

The largest excess heat production per unit of surface area was from the R37 reactor, which was made from SUS304, and exposed to air. The second largest was SUS304 R8 reactor, with the vacuum activated surface of the nickel mesh. Next was the Ni mesh in R36. The activation treatment was SUS304. R35 is made of SUS304 and it has a Ni net, but it has no electrodes for activation treatment, and no excess heat was observed from this reactor. The latest rector, R40, is closest to reactor R37 in terms of energy production.

The test results are summarized in Table 3. The reactors are listed in descending order, with the largest excess heat generation and the easiest heat to produce (with lowest activation energy) at the top. The 9th and 10th columns on the right side show the activation energies and frequency factors of the reactions, respectively. The frequency factor here is the amount of heat at 1/T = 0. The R37 reactor has a very large value. Activation energies do not differ significantly between tests, being −0.27 to −0.29 eV/K/atom.

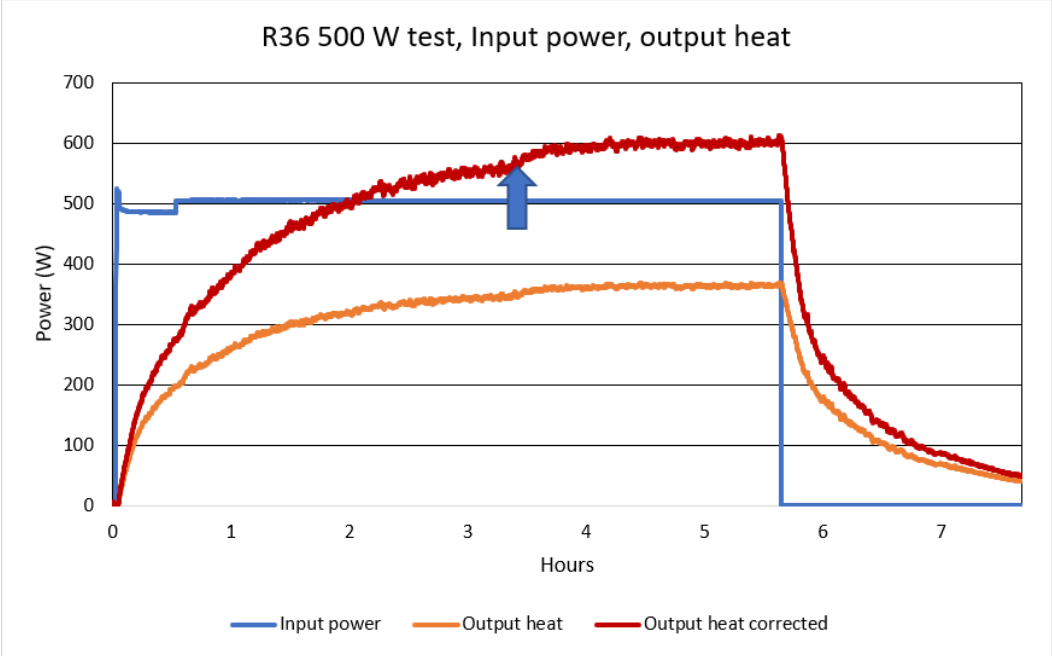

Figure 16. R36 test at 500 W. Output heat is 363 W uncorrected or 598 W corrected. The blue arrow points to the effect of an abrupt 1.4°C fall in inlet temperature.

9. Material Preparation

The reaction occurs with stainless steel that has been stressed to produce defects at the surface layers. The following steps are needed to produce the effect:

1. Excess heat is produced when stainless steel or nickel surfaces are cleaned and roughened to produce defects at near surface layers, and then exposed to hydrogen or air.
2. The reaction takes place not only when the reactor is exposed to hydrogen gas, but also when it is in open air.
3. When the temperature exceeds 350°C, the metal surface oxidizes, which retards the reaction. It is better to exclude air from tests at such high temperatures.
4. When the reactor is filled with H_2 or D_2 gas, the reaction occurs at temperatures above 350°C.
5. Hydrogen in the metal surface layer reacts both in air and at a low vacuum.
6. In the tests with pressurized reactors, the pressure has been 10 to 50 MPa. The reaction would probably work better at higher pressure, 100 to several kilopascals, because the results show the reaction attenuates whether pressure is high or low.
7. The amount of heat generated depends more on temperature than on pressure, and increases exponentially with temperature.
8. With a closed reactor is exposed to hydrogen, excess heat is obtained by first cleaning the reactant nickel surface by irradiating it hydrogen ions from an electrical discharge.

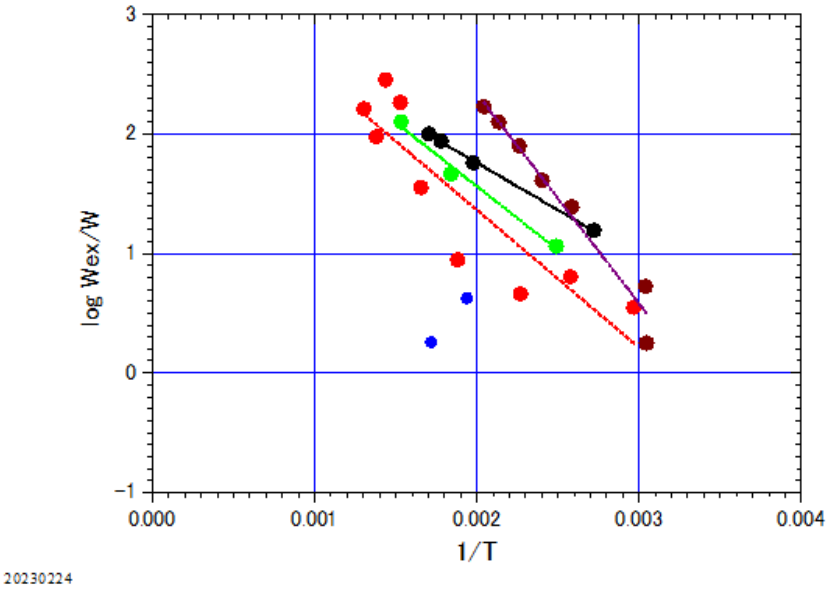

Figure 17. Arrhenius plot. The horizontal axis is reciprocal of absolute temperature, 1/T. The vertical axis is logarithmic excess heat per unit of area. The blue dots for R35 show no excess heat.

9. Electrical discharge treatment in a low vacuum is an effective way to make an extremely clean metal surface. We presume this produces a hydrogen-active surface that intensifies the reaction. We presume that nickel or stainless steel will react if it has this kind of hydrogen-active surface.
10. The most necessary condition is to compress and stress the metal surface, to form many defects near the surface (estimated to be at several micrometers). The defects must have a certain size (estimated at several nanometers) to create an optimum reaction site. Buffing is best for this. Electropolishing is not suitable because it removes the processed layer. Emery polishing is also unsuitable because it removes the processed layer. A rotating buffer of the kind used to polish metal is most suitable. No reaction occurs without this treatment, and without the defects.

10. Conclusions

This data shows that even a simple SUS reactor, if the surface treatment is suitable, can produce excess thermal energy exceeding the input. It can also be seen that the excess heat increases exponentially with temperature. Excess heat generation tests were conducted using four types of samples and reactors with different treatment methods.

The following reactors produced heat:

1. The R37 straight tube reactor with only stainless-steel surface and no electrical discharge produces excess heat.
2. The R8 cross-shaped reactor with a nickel mesh inside produced heat even after discharge treatment.

3. The R36 cross-shaped reactor with a Ni mesh on the inside, and nothing on the surface, where the Ni mesh was treated with electric discharge.
4. The R35 small reactor did not produce heat. This reactor has a nickel mesh, but no discharge treatment was applied, because this reactor has no discharge electrode.

Excess heat is produced when stainless steel or nickel surfaces are cleaned roughened to produce defects at near surface layers, and then exposed to hydrogen or air.

Acknowledgements

The authors would like to thank the following people and companies for their assistance in the writing of the paper, testing, analysis, and analysis.

We would like to thank Sanshu Kogyo Co., Ltd. for confirming the excess heat with the reactor and measurement system which they built.

We would like to thank Dynax Industries Co., Ltd. for confirming the excess heat in the furnace body built by Mizuno with a high-temperature thermostatic chamber they built themselves, and for analyzing the data.

We would like to express our sincere gratitude to Jean-Paul Biberian of the University of Marseille for performing a preliminary confirmation of excess heat generation from a reactor provided by Mizuno.

We would like to express our deep gratitude to Murata Manufacturing Co., Ltd. for building a transpiration heat measurement system at a new research site and for confirming the excess heat of 200 W. This was more than three times the input and was maintained for several weeks, from the seven reactors provided by Mizuno.

References

[1] Fleischmann, M., S. Pons, and M. Hawkins, *Electrochemically induced nuclear fusion of deuterium.* J. Electroanal. Chem., 1989. **261**: p. 301 and errata in Vol. 263.

[2] Fleischmann, M., et al., *Calorimetry of the palladium-deuterium-heavy water system.* J. Electroanal. Chem., 1990. **287**: p. 293.

[3] Fleischmann, M. and S. Pons, *Some comments on the paper Analysis of experiments on the calorimetry of LiOD-D2O electrochemical cells, R.H. Wilson et al., J. Electroanal. Chem. 332 1992 1.* J. Electroanal. Chem., 1992. **332**: p. 33.

[4] Fleischmann, M. and S. Pons, *Calorimetry of the Pd-D2O system: from simplicity via complications to simplicity.* Phys. Lett. A, 1993. **176**: p. 118.

[5] Fleischmann, M., S. Pons, and D.R.O. Morrison, *Reply to the critique by Morrison entitled 'Comments on claims of excess enthalpy by Fleischmann and Pons using simple cells made to boil.* Phys. Lett. A, 1994. **187**: p. 276.

[6] Jones, J.E., et al., *Faradaic efficiencies less than 100% during electrolysis of water can account for reports of excess heat in 'cold fusion' cells.* J. Phys. Chem., 1995. **99**: p. 6973.

[7] Mizuno, T., et al., *Anomalous heat evolution from a solid-state electrolyte under alternating current in high-temperature D_2 gas.* Fusion Technol., 1996. **29**: p. 385.

[8] Mizuno, T., et al., *Anomalous gamma peak evolution from SrCe solid state electrolyte charged in D_2 gas.* Int. J. Hydrogen Energy, 1997. **22**: p. 23.

[9] Mizuno, T., et al., *Neutron Evolution from a Palladium Electrode by Alternate Absorption Treatment of Deuterium and Hydrogen.* Jpn. J. Appl. Phys. A, 2001. **40**(9A/B): p. L989–L991.

[10] Mizuno, T., et al., *Anomalous isotopic distribution of elements deposited on palladium induced by cathodic electrolysis.* Denki Kagaku oyobi Kogyo Butsuri Kagaku, 1996. **64**: p. 1160 (in Japanese).

[11] Neuville, S., *Perspective on Low Energy Bethe Nuclear Fusion Reactor with Quantum Electronic Atomic Rearrangement of Carbon.* J. Condensed Matter Nucl. Sci., 2017. **23**: p. 91–116.

[12] Alabin, K., et al., *Isotopic and Elemental Composition of Substance in Nickel–Hydrogen Heat Generators.* J. Condensed Matter Nucl. Sci., 2018. **26**: p. 32–44.

[13] Beiting, E., *Investigation of the nickel-hydrogen anomalous heat effect*. 2017, Report No. ATR-2017-01760: The Aerospace Corporation.
[14] Hagelstein, P.L. and I. Chaudhary. *Excitation transfer and energy exchange processes for modeling the Fleischmann-Pons excess heat effect*. in *ICCF-14 International Conference on Condensed Matter Nuclear Science*. 2008. Washington, DC.
[15] Mizuno, T. and J. Rothwell, *Experimental procedures for excess heat generation from cold fusion reactions in Cold Fusion Advances in Condensed Matter Nuclear Science*, J.P. Biberian, Editor. 2020, Elsevier https://www.elsevier.com/books/cold-fusion/gromov/978-0-12-815944-6.
[16] Bartl, J. and M. Baranek, *Emissivity of aluminium and its importance for radiometric measurement.* Measurment Science Review, 2004. **4**.
[17] *Gase und Kohlenstoff in Metallen*, ed. E. Fromm and E. Gebhardt. 1976, Berlin: Springer Verlag.
[18] Ohmi, T. and T. Shibata, *Ultra Clean Technology Its Impact on High Integrity Ultra-Thin Gate Oxide Formation*, in *SEMICON/korea Technical Symposium 93*. 1993. p. 195-202 https://kaken.nii.ac.jp/ja/grant/KAKENHI-PROJECT-05237204/.
[19] Sazaki, H., *Next-Generation Energy System to Produce Hydrogen from Water Using Mechanical Energy (in Japanese)*, in *2nd Industrial Infrastructure Creation Research Report.* 2013, The Canon Foundation https://jp.foundation.canon/common/pdf/aid_awardees/2/k2_5_saziki_security.pdf.